WORLD CONFERENCE ON TIMBER ENGINEERING 2025
BRISBANE, AUSTRALIA
Advancing Timber for the Future Built Environment

PREFABRICATED MASS TIMBER HYBRID SYSTEMS: INVESTIGATION ON ADOPTING CNC-MADE CARPENTRY JOINTS TO INDUSTRIALIZED LONG-SPAN FLOORS

Yue Diao[1], Cristiano Loss[2]

ABSTRACT: Automation in Construction 4.0 encompasses the use of robotics, machinery and automated processes to enhance production efficiency and manufacturing accuracy. While automation in the design and assembly of timber structures has been extensively discussed in the field of architecture, most implementations are limited to small-scale demonstration projects. Modularized prefabricated timber assemblies can benefit greatly from automation; however, challenges persist in the proper design of connection systems, especially for large-scale structural systems. Despite current manufacturer capabilities in producing prefabricated wall assemblies, there remains an opportunity to develop higher-level prefabricated assemblies in factory settings. CNC-made carpentry joints are optimal candidates for assessing this design problem. Integrated design is needed to meet structural demands in modern constructions and manufacturing restraints in CNC machinery. However, most discoursed designs fail to use a standardized digital environment. This paper addresses these gaps by proposing a workflow for the development of innovative CNC-made carpentry joints for use in long-span CLT-glulam composite flooring systems, testing such a digital environment via the structural design and fabrication of full-scale bamboo tenon-type shear connectors. This innovation highlights the potential for integrating automation in the future mass production of carpentry joints for prefabricated mass timber assemblies.

KEYWORDS: CNC-made Carpentry Joints, Standardized Timber Assemblies, Design for Manufacturing and Assembly, Bamboo Joints

1 – INTRODUCTION

Wood, as a renewable and recyclable material, shows promising attributes for sustainable construction. Wood products and their structural assemblies can be cost-effective if they are delivered in a cost- and time-efficient manner. Automation technology combined with digitalization forms the foundation for manufacturers transitioning to Industry 4.0 [1]. During this transformation, wood machinery manufacturers focusing on advancements in technology for customized wood joinery are poised to enter larger markets such as the construction industry [2]. The market has embraced highly customized free-form timber structures for their aesthetic appeal; however, these projects are not viable solutions for addressing housing demand due to the lack of skilled professionals with a multidisciplinary background and labour shortages [3].

1.1 AUTOMATION IN TIMBER STRUCTURES

The primary sources for free-form timber structures are small wood units or wood logs with unique geometric features. Robotic arms are the standard automation tools used in processing these elements due to their higher flexibility. Automatic assembly process programs were developed for common fasteners such as screws [4]. A research team from EPFL focused on the automated assembly process for new wood products [5]. However, advancements in using automation technology for the implementation of large-scale mass timber construction have yet to reach full maturity [6]. Therefore, research is needed to update prefabricated timber assembly solutions using automation technology in wood product factories driven by housing demand worldwide. In this

[1] Yue Diao, Ph.D. Candidate, Sustainable Engineered Structural Solutions Laboratory, Department of Wood Science, University of British Columbia, Canada, yuediao@mail.ubc.ca

[2] Cristiano Loss, Associate Professor, Sustainable Engineered Structural Solutions Laboratory, Department of Wood Science, University of British Columbia, Canada, cristiano.loss@ubc.ca

https://doi.org/10.52202/080513-0149

context, this study investigates the development of long-span T-section CLT-glulam composite floors assembled with CNC-made bamboo tenon-type connectors. All employed materials were taken with commercial sizes and standard mechanical properties.

1.2 CNC WOOD MACHINES

Mass timber manufacturing production lines are typically equipped with specialized CNC machines for product profiling before their final finishing and packaging. Equipment such as Hundegger [7], Biesse [8], and Techno Wood [9] are specifically designed for mass timber products. These CNC machines are outfitted with a variety of cutting tools, typically categorized as circular saw blades, end mills, cutters, and drills. These tools enable the machines to perform essential woodworking operations. Customized cutters can be made on demand.

The feed-in mechanisms of these machines can accommodate full-sized panels or large glulam beams. For instance, the Hundegger ROBOT series features feed-in and outfeed racks extending up to 10 meters and are equipped with a hydraulic lift table, making them suitable for the profiling of long-span glulam beams. Gantry machining centre, on the other hand, are often designed to process larger timber members with the capability to handle panels of considerable dimensions [10].

Despite their versatility, these machines are predominantly used for cutting timber-frame joints on glulam or profiling CLT panels for prefabricated wall systems [11]. For the fabrication of wood joinery, particularly tenon joints, the most commonly available CNC machines in wood product manufacturing are those developed by HOMAG [12]. Widely utilized in the furniture industry for producing joint systems, HOMAG CNC machines offer high precision and automation, particularly for smaller-scale joints. Given the advanced level of automation and the proven reliability of these machines in furniture production, they present a promising opportunity for manufacturing structural-grade carpentry tenons tailored for use in mass timber structures.

2 – WORKFLOW FOR DEVELOPING CNC-MADE CARPENTRY JOINTS

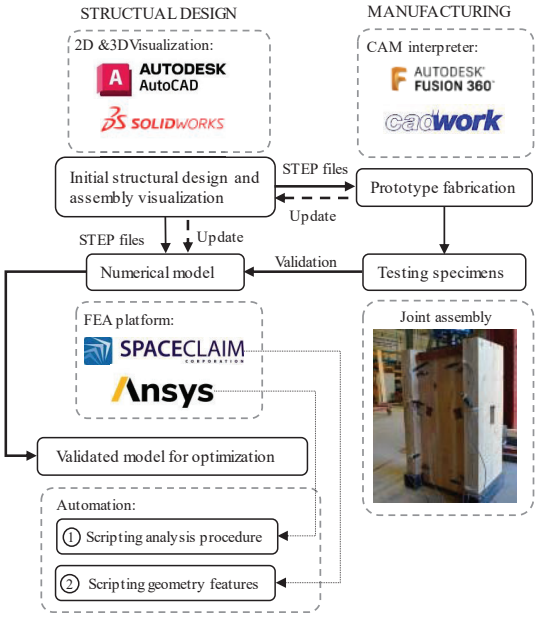

Figure 1 Workflow for the wood joints development

Fig. 1 illustrates the workflow used in the development of a CNC-made carpentry joint specific for CLT-glulam structural assemblies. With specific reference to composite flooring applications, the design process went through an iterative updating loop, starting from estimating performance demands, then incorporating machinery capability and including operations for a quick system-assembly process, and then constraining to system-level estimated performance. 2D and 3D drawings of the prototyped tenon-type joint were created in a standardized CAD environment, with data properties shared in the form of STEP files, which were read by CAM software. These data files were imported into structural analysis software to define the geometry of a finite-element (FE) model. The workflow was checked against a carpentry joint prototype that has been tested under lateral loading. Test results from the series assembly were then used to validate the FE model accuracy in predicting the load-slip behaviour of carpentry joints. The script of the numerical model was then expanded to study the effects of design changes and boundary conditions on the mechanical response of the prototyped carpentry joints.

2.1 STURCTURAL DESIGN

Long-span composite floor systems, combining cross-laminated timber (CLT) slabs with glulam beams, offer structural efficiency by reducing floor height and material usage while enhancing aesthetic appeal through exposed wood. These systems are ideal for open-plan

https://doi.org/10.52202/080513-0149

public and mixed-use buildings, providing design flexibility and promoting occupant well-being.

In line with these objectives, this study focuses on an efficient, modular, long-span T-section composite floor system consisting of a 3-ply CLT slab connected to 12-meter glulam beams. The adaptation of the carpentry joint serves as a connection system, enhancing both structural performance and ease of assembly. The structural members for this composite floor have been modularized, as discussed in [13]. The modular design optimizes cross-sectional dimensions and material arrangement, ensuring material-saving. The modular design also accounted for dimensional staggering due to the wood product manufacturing processes. The optimized structural dimensions derived from this modularized design are listed in Table 1 and represent the minimum product dimensions needed in the original modular layout. However, the final product selection was adjusted to the most readily available material sizes based on the inventory of a local producer in 2023.

Table 1: Mass Timber Products Dimensions

Product type	**Modular design dimensions**		**Supplier-provided product dimensions**	
	Width (mm)	***Thickness /Depth (mm)***	***Width (mm)***	***Thickness /Depth (mm)***
CLT panel	1200	105	2400	105
Glulam	175	380	268	453

Referring to Table 1, the CLT panel provided is made of a spruce-pine-fir combination, graded E1M5, as developed by the manufacturer in accordance with CSA O86-19 and ANSI/APA PRG 320 [14-15]. The modular design of the CLT panel is derived from a standardized 2.4-meter-wide 3-ply panel. The glulam is Douglas fir, graded 24f-EX as per CSA O122-16 [16]. For prototyping purposes, a glulam section with a width of 268 mm and a depth of 453 mm was selected.

The design of the traditional carpentry joint for the CLT-glulam composite flooring system was informed by structural requirements [13,17], available material sizes (Table 2), and ease of assembly. Parallel strands bamboo (PSB) was selected as the tenon material due to its densification process, which provides higher stiffness, material stability, and bearing capacity. The peg material was then chosen between PSB and laminated bamboo lumber (LBL), considering their machinability in wood workshops and CNC machines. The dimensions of the structural engineered bamboo products listed in Table 2 are based on commercially available options from MOSO International [18]. Notably, LBL has two distinct cross-sectional orientations, namely flatwise and edgewise. The depth and width dimensions used in this study are illustrated in Fig. 2. PSB is treated as a transversely isometric material as its cross-sectional properties are uniform in all directions. The design specifications for the tenon and peg are also provided in Table 2.

Fig. 3 presents the original prototype, crafted as a tenon-peg system. This design was developed based on consultation with technicians specializing in wood processing and machining.

Table 2: Specifications of commercialized bamboo products and designed tenon and peg dimensions

Product type	**Beam dimensions (mm)**			
	Length	***Depth***		***Width***
PSB beam	2440	120		72
LBL beam	2440	120		72
Subassembly	**Design dimensions (mm)**			
	Insert depth	***Length***	***(Tapered)***	***Width***
Tenon	154	115	55	69
Peg	268	69	59	55

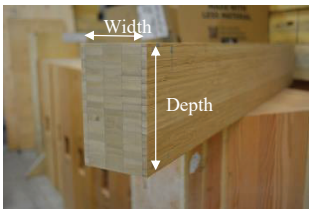

Figure 2 Cross-sectional layouts of LBL

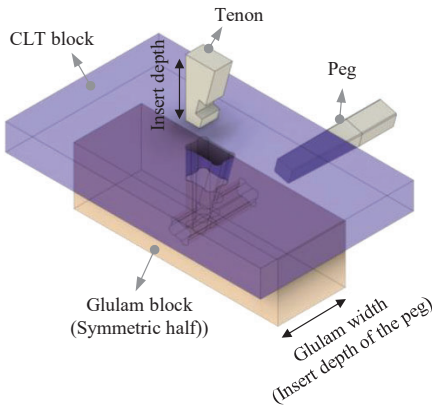

Figure 3 Designed tenon-peg connection system for CLT-glulam joint assembly

https://doi.org/10.52202/080513-0149

2.2 DESIGN FOR MANUFACTURING

The prototype was manufactured in-house with the technical assistance of technicians from the Center for Advanced Wood Processing workshop (CAWP) at the University of British Columbia (UBC). The milling of CLT and glulam beams was performed using a Hundegger ROBOT drive CNC timber processing centre customized for lab environments (Fig. 4(a-d)), whereas tenon and peg were fabricated using the Homag 5-axis Centateq P-310 processing centre (Fig. 5). Each machine has specific working space limitations as is listed in Table 3.

Note that two CNC machines have different feed mechanisms: the Hundegger processes materials by moving them along a track, whereas the Homag operates on stationary pieces. Consequently, the material requirements differ depending on the machine.

In addition, the width of the CLT panel was reduced to 600 mm to ensure compatibility with the Hundegger machine and to localize the study to a single joint. Larger CNC machines could accommodate broader dimensions, which would eliminate this restriction.

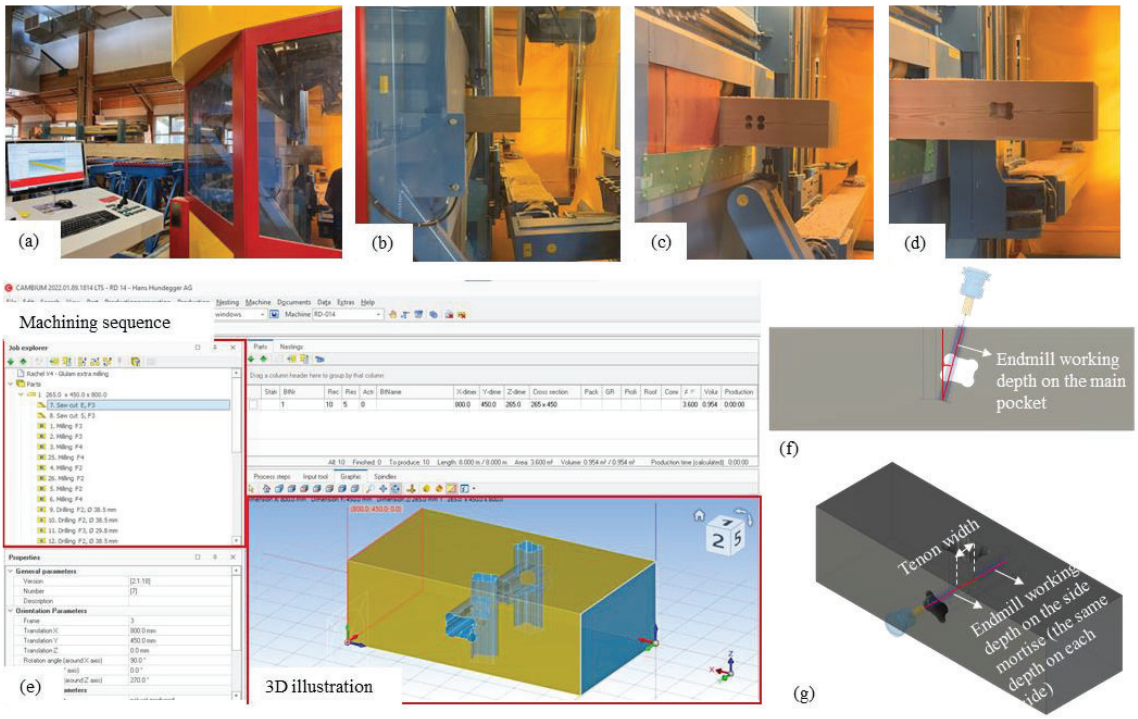

Figure 4 Hundegger CNC timber processing centre: (a-d) glulam processing: operation centre (Cambium), sawing, drilling and milling; (e) Cambium programming interface; (f-g) endmill working depths for different mortise cuts on glulam

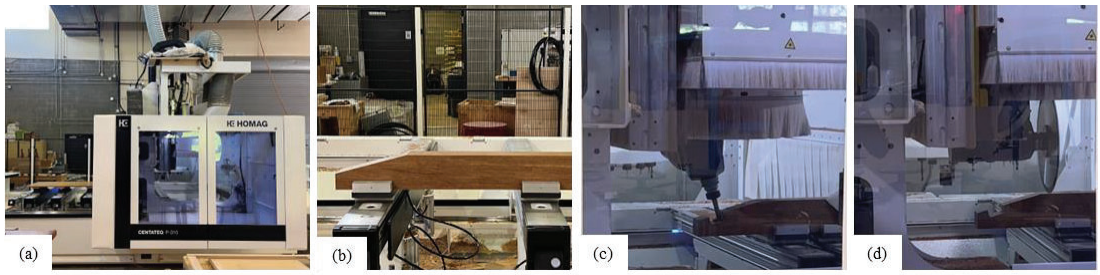

Figure 5 Homag processing centre: (a) setup of the processing centre; (b-d) tenon processing: tapered surface, milling and cutting to length

https://doi.org/10.52202/080513-0149

Table 3: CNC machining specifications

CNC machine specifications	**Material dimensions (mm)**	
	Width	650
Hundegger ROBOT Drive	Thickness	300
	Thickness	200
Homag Centateq P-310	Length	3300
End mill selection		
Mortise locations	***Working length***	***ϕ***
Glulam main pocket	160	40
Glulam side mortise/CLT panel	120	30

Fig. 4(e) illustrates the CNC programming interface, Cambium, which outlines the processing sequence alongside a 3D illustration of a glulam block with two tenon-peg systems. For local machining of mass timber products, challenges arose when creating mortise cuts in the glulam beams. This process requires two-axis milling to create both a pocket (Fig. 4(f)) and a side mortise (Fig. 4(g)). The selection of endmills, also listed in Table 3, was guided by supplier specifications, with key considerations including endmills' working length and diameter. The total manufacturing time for a double-shear plane glulam block used in testing is approximately 25 minutes. However, for flooring applications, this time is expected to be reduced by more than half since each flooring segment requires only one shear plane. This reduction is primarily due to decreased milling, tool changes and robotic arm travelling time.

In contrast, milling mortise cuts in CLT panels is more straightforward, as it involves a simple "through-and-through" cut. For thicker panels, the cut can be completed by milling from both sides.

As illustrated in Fig. 5 (b-d), the manufacturing of the tenon involves (i) cutting the slope and length and (ii) milling the mortise cut for the peg. Since the tenon is directly profiled from the bamboo beam, the only constraint is ensuring the material fits within the working table dimensions. Once the material is properly aligned and secured, the total fabrication process takes less than 5 minutes.

2.3 PROTOTYPING AND FINALIZING

The manufactured PSB tenon is shown in Fig. 6(a). Following the initial manufacturing and a test fit of the first assembly, a final adjustment was made to the peg, as depicted in Fig. 6(b) of a LBL peg. This adjustment involved tapering two surfaces of the peg to ensure a precise fit. The assembly process, carried out in a controlled laboratory environment, is illustrated in Figs. 9(c) and 9(d), with specific reference to a double-shear joint configuration. Specifically, the finalized experimental specimens were designed to feature two one-meter-long CLT panels and a single glulam block, joined by two sets of tenon-peg connectors on each shear plane. While this double-shear configuration does not replicate actual flooring applications, it was chosen to improve balance and stability during push-out shear tests and to simplify the prototyping process. It also avoids the added complexity of single-shear plane specimens [19].

A mallet, a commonly used tool in woodworking workshops, was employed for the installation.

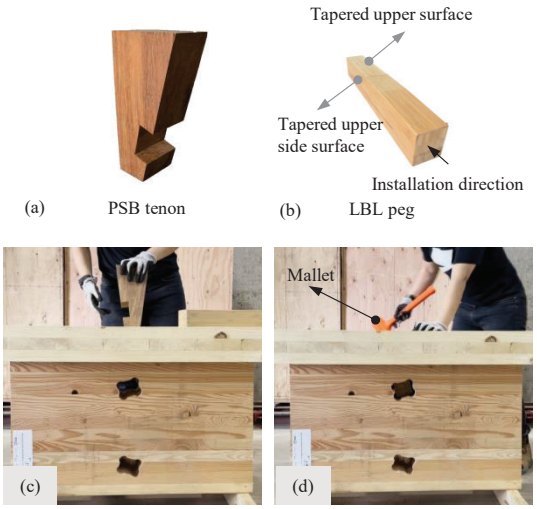

Figure 6 Prototyping of the PSB-LBL testing group: (a) PSB tenon, (b) LBL peg, (c) insertion of the tenon, (d) insertion of the peg

3 – PUSH-OUT SHEAR TESTS

Push-out shear tests were conducted to characterize the mechanical properties of the proposed bamboo tenon-type joint for CLT-glulam composite flooring applications. Two specimen groups were evaluated, distinguished by the type of pegs utilized. Group 1 incorporated PSB pegs, while LBL pegs were employed in Group 2. Both groups featured PSB tenons. Each group consisted of 6 replicates subjected to testing. Moisture content (MC) measurements for both cross-laminated timber and glulam were conducted in a controlled laboratory setting at room temperature using a moisture meter. The CLT panels displayed moisture content values ranging from 10.2% to 11.4%, with an average of 10.6%. The glulam subassemblies showed

moisture content between 9.5% and 10.3%, averaging 9.9%.

The mechanical tests were conducted at room temperature in the High Head Wood Mechanics Laboratory at UBC. Given the absence of specific guidelines for carpentry joints in current testing standards, the monotonic loading procedure outlined in ASTM D1761-20 [20] was used. A double-shear plane push-out test configuration was selected to ensure greater stability and more uniform load distribution across both shear planes.

The initial stiffness as per ASTM D1761-20 was calculated using Equation (1).

$$k = \frac{0.4F_{max} - 0.1F_{max}}{\Delta_{0.4} - \Delta_{0.1}} \quad (1)$$

Where 0.4 F_{max} and 0.1 F_{max} represent 40% and 10 % of the load-carrying capacity of one joint; $\Delta_{0.4}$ and $\Delta_{0.1}$ are the corresponding slip per joint.

The test setup for the specimen in the double shear plane configuration is shown in Fig 7. The applied load and total displacement were collected from the load cell, while the relative slip was obtained from transducers 01 and 02, mounted adjacent to the pegs. Additionally, 4 transducers were mounted at the top and bottom of the specimen to monitor the out-of-plane movement of the CLT panel. The recorded out-of-plane displacements were subtracted from the total slip to attain the actual slip between the CLT panel and the glulam subassembly.

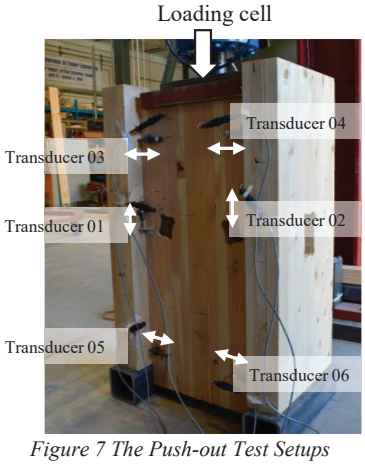

Figure 7 The Push-out Test Setups

The load-carrying capacity per joint was determined by dividing the peak value reached during the test by 2 due to the symmetrical design of the push-out tests.

4 – RESULTS AND DISCUSSION

4.1 MEASURED TOLERANCE

In this tenon-peg design, two primary sources of gaps were identified as contributing to the initial slip: the manufacturing tolerance of the glulam mortise and the adjusted tapered peg. Measurement locations for the glulam mortise are shown in Fig. 8, with corresponding measurement results detailed in Table 4. It is important to note that because the peg is specifically designed to fix the tenon's position within the mortise, tolerance on the side mortise of the glulam was not considered in this study. Instead, the assembly gaps introduced by the tapered peg surfaces were accounted for, as illustrated in Fig. 9.

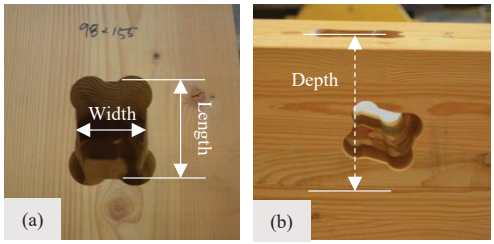

Figure 8 Measurements on the glulam mortise (main pocket)

Table 4: Design and measurement of the glulam mortise cut for the tenon

Location	Design Value	Measured Average	Discrepancy
Glulam mortise			
Depth (mm)	154.00	156.04	2.04
Length (mm)	96.24	97.31	1.07
Width (mm)	69.00	69.59	0.59

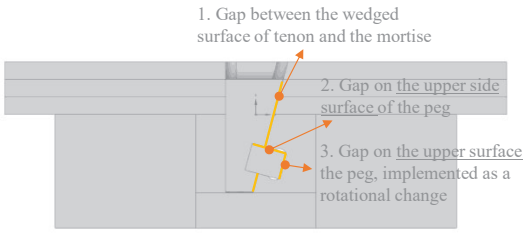

Figure 9 Gaps' locations in consideration

https://doi.org/10.52202/080513-0149

4.2 MECHANICAL PROPERTIES

The load-carrying capacities per joint, estimated based on the test series of each group, are statistically represented in the boxplot of Fig. 10(a). The boxplot illustrates the median (black line in the middle of the box), the mean (red diamond), and individual data points (black dots). Outliners, defined as values exceeding 1.5 times the interquartile range, are marked with crosses.

The PSB-PSB group exhibited an average load-carrying capacity of 111 kN, with values ranging from 96 kN to 133 kN. In contrast, the PSB-LBL group had a slightly lower average capacity of 106 kN, ranging from 92 kN to 120 kN, with two identified outliers indicating greater variability. Despite the overlapping ranges, the PSB-PSB group consistently achieved higher load capacities, suggesting improved performance under shear loads.

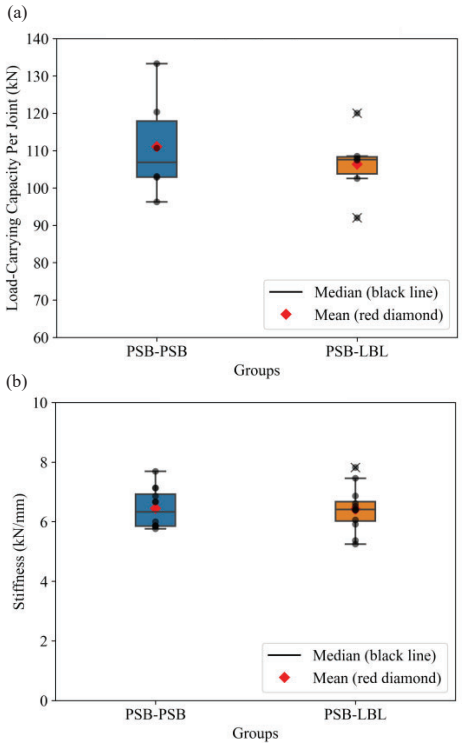

Figure 10 The statistical results: (a) Load-Carrying Capacity Per Joint, (b) Stiffness per joint

The initial stiffness of the joints is illustrated in Fig. 10(b) as boxplots for both groups. Both the PSB-PSB and PSB-LBL groups recorded the same average stiffness of 6.4 kN/mm; however, the data distribution differs between the groups. The PSB-PSB group displays a wider interquartile range (5.9-6.9 kN/mm), indicating greater variability within the central data cluster. In contrast, the PSB-LBL group shows a narrower interquartile, ranging from 6.0 to 6.7 kN/mm, but the presence of the outliner and the spread of the whiskers suggest higher variability in stiffness at the extremes.

These boxplots indicate that the PSB-LBL group exhibits less consistent performance in both load-carrying capacity and stiffness compared to the PSB-PSB group, whose results are more tightly clustered. Given that both groups were designed and fabricated using the same workflow, materials from the same batch, and identical testing setups, the observed variations can be attributed primarily to the difference in peg material. The inherent variability in the material properties of the LBL pegs likely affects local stress distribution, contributing to the observed inconsistencies in joint performance.

5 – DESIGN AND TOLERANCE EFFECTS ON INITIAL JOINT PERFORMANCE

Although CNC machining ensures high precision in the fabrication of timber elements, discrepancies between the design and actual dimensions still arise. These variations stem primarily from a combination of factors in machining, including milling speed, local vibrations, tool deflection and slight material movement during processing. Additionally, wood's natural grain and internal stresses may cause minor shifts in local areas.

Beyond fabrication-induced variations, intentional gaps must also be incorporated during assembly to facilitate ease of fitting. Unlike metalworking, which demands extremely tight tolerances, woodworking typically allows for tolerances in the range of ±2 mm for large-scale operations and ±0.5 mm for smaller machines. Well-designed carpentry joints, particularly interlocking systems like the tenon-peg joint examined in this study, can effectively accommodate these tolerances and thus enhance structural integrity.

While minor deviations in an individual tenon and/or mortise do not significantly impact the load-carrying capacity of a joint, they contribute to initial slip, thereby reducing its elastic stiffness. To systematically evaluate the influence of these tolerances on joint performance, a parametric study was conducted, treating the gaps as independent variables.

A finite element model was employed for the parametric study, built using an imported STEP file. The wood products and LBL were modelled as orthotropic materials within their elastic regions, incorporating

isotropic kinematic hardening and Hill's criterion to define their yielding behaviour. PSB was modelled as a transversely isotropic material with its plasticity defined in the same manner as the other materials. Specific values for material properties, meshing methods, and contact region definitions were sourced from [17]. Boundary conditions mirrored those used in the monotonic push-out tests. Simulation results were validated against the average experimental results of the PSB-LBL specimens, showing strong agreement in its initial stiffness.

The parametric study was conducted using an orthogonal experimental design to investigate the influence of contact gaps on joint performance. The factors analysed included gaps on the tenon wedged surface, the upper side, and the upper surface of the peg. Three levels of tolerances and/or gaps for each factor are specified in Table 5. The simulation results are presented in Fig. 11, where the test results are shaded in yellow. The remaining curves represent the parametric simulations, all running up to a 5 mm slip to focus on the tolerance effects during the initial stage of the load-slip relationship.

Two key observations were made from Fig. 11. First, by examining the load at a slip of 5 kN (horizontal line 1), the curves can be categorized into two groups: one group exhibits no significant initial slip, while the other shows a two-segment behaviour, indicative of a tolerance-induced slippage phase. Second, from the 5 mm slip mark (vertical line 2), the reaction load per joint falls into three distinct ranges depending on the combination of tolerances: 25–30 kN, approximately 35 kN, and over 40 kN. These observations highlight the significance of tolerance combinations on joint performance, particularly in the initial stages of load application.

Table 5 Orthogonal Experimental Design

Model Name	**Contact Gaps Locations**		
	Tenon	***Peg***	
	Wedged surface	***Upper side***	***Upper surface***
	(mm)	(mm)	(Rotational degree)
TO1	2	2.5	0.2
TO2	2	1.2	0.1
TO3	2	0	0
TO4	1	2.5	0.1
TO5	1	1.2	0
TO6	1	0	0.2
TO7	0	2.5	0
TO8	0	1.2	0.2
TO9	0	0	0.1

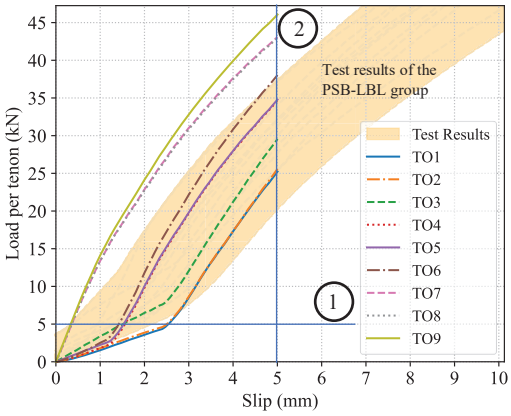

Figure 11 The load-slip results of modelling with variant gaps in the joint model

To further quantify the influence of these tolerances on joint performance, an analysis of variance (ANOVA) was conducted. The first focused on slip responses at a load of 5 kN, while the second evaluated the reaction force at a slip of 5 mm. The results of ANOVA at two responses are listed in Table 6.

Table 6: ANOVA Results

ANOVA results at response 1				
Contact gaps	***Sum of Squares***	***df***	***F-value***	***PR(>F)***
Tenon				
Wedged surface	5.39	2	26.33	0.0366
Peg				
Upper side	0.33	2	1.59	0.3861
Upper surface	0.22	2	1.07	0.4838
Residual	0.20	2		
ANOVA results at response 2				
Contact gaps	***Sum of Squares***	***df***	***F-value***	***PR(>F)***
Tenon				
Wedged surface	446.16	2	2278.38	0.0004
Peg				
Upper side	24.62	2	125.70	0.0079
Upper surface	0.31	2	1.57	0.3890
Residual	0.20	2		

The ANOVA analysis results demonstrate that the contact gap on the wedged surface of the tenon has a statistically significant effect on joint performance at both response collection points. At the first response point, corresponding to the slip at 5 kN, the p-value (column PR(>F)) was 0.0366, indicating a significant

https://doi.org/10.52202/080513-0149

influence of the tenon wedged surface gap on the initial slip behaviour. Similarly, at the second response point, corresponding to the reaction force at 5 mm slip, the p-value is 0.0004, further confirming the critical role of this factor in determining the joint's mechanical performance. In contrast, neither the upper side nor the upper surface gaps on the peg exhibited statistically significant effects under the experimental conditions, with p-values well above 0.05 at both response points.

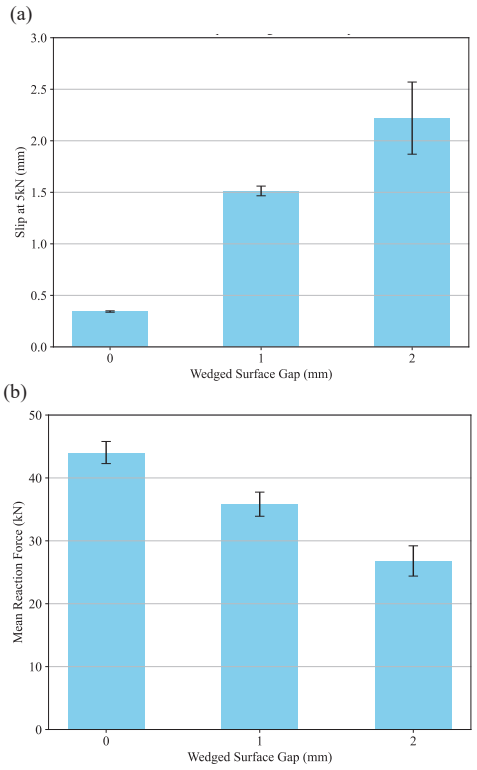

Figure 12 Mean values of each wedged surface gap: (a) mean slip at 5 kN; (b) mean reaction force at a slip of 5 mm

Figs. 12(a) and 12(b) present the mean values at two response variables influenced by the wedged surface gap: (1) mean slip at 5 kN and (2) mean reaction force per joint at 5 kN. These plots provide a clearer understanding of the effect of the wedged gap, identified as the most significant factor from the ANOVA analysis discussed earlier.

For response 1 (mean slip at 5 kN) shown in Fig. 12(a), an increase in the wedged surface gap leads to a corresponding rise in slippage. Specifically, when the gap increases to 1 mm, the mean slip exceeds 1 mm, reaching approximately 1.5 mm. A further increase to a 2 mm gap results in a slip of 2.2 mm. It shows that while the absolute slippage increases with the gap size, the rate of increase diminishes, suggesting a potential threshold beyond which additional gap increments have a reduced effect. The error bars, representing the standard error of the mean, indicate greater variability in slip as the wedged gap widens, highlighting increased inconsistency in joint performance under larger gaps.

For response 2 (mean reaction force per joint at 5 kN) depicted in Fig. 12(b), the mean reaction force decreases as the wedged surface gap increases. This trend is consistent with the initial observations from the load-slip curves in Fig. 11, underscoring the critical influence of the wedged gap on joint load resistance. While the error bars show a slight increase in variability with larger gaps, this variation is less pronounced compared to the slip response. This suggests that although the wedged gap significantly affects both responses, its impact on load-carrying capacity is more consistent than on slippage.

These findings reinforce the decisive role of the wedged surface gap in influencing joint performance. The increased slip and reduced reaction force with larger gaps are likely due to altered stress distribution and reduced contact efficiency within the joint. The variability trends observed further suggest that controlling the wedged gap during manufacturing could improve the consistency and reliability of joint behaviour in structural applications. Moreover, tighter control of joint tolerances not only enhances stiffness but also reduces variability, which is critical for the overall performance of composite flooring systems. Improved joint stiffness contributes to better load distribution and reduced deflections, directly impacting the system's serviceability performance.

On the other hand, the gaps on the peg surfaces can be incorporated as a design feature to facilitate assembly without significantly influencing the joint's mechanical behaviour. The parametric study thus provides actionable insights, suggesting that focusing on the precision of tenon-mortise contact surfaces is critical for improving joint performance, while tolerances on the peg can remain more flexible to enhance ease of assembly.

In the context of standardization and the potential development of future codes for digitalized carpentry joints, the proposed workflow represents a significant contribution. Grounded in structural design principles, it leverages commercially available products and CNC technologies to precisely control performance-influencing factors. This approach not only facilitates

the generalization of digitalized carpentry joints but also allows for their adaptation to a wide range of structural systems. Additionally, the workflow provides a systematic method for identifying and addressing real-world variables, such as material deviations, CNC machining tolerances, and design-for-assembly considerations.

6 – CONCLUSION

This study has demonstrated the potential of implementing CNC-made carpentry joints via a standardized digital environment. A workflow for the development of a new generation of carpentry joints for use in prefabricated hybrid timber floors has been presented and its design procedure has been tested.

To further inform the industry, a parametric study investigated the effects of manufacturing tolerances on the structural performance of these joints. The ANOVA analysis, based on an orthogonal experimental design, identified the most critical tolerance to be the contact gaps between the tenon and mortise in the direction parallel to the shear force. This finding underscores the importance of precise fabrication in specific local areas and assembly to ensure optimal joint performance.

Future research should focus on optimizing the joint arrangement within the flooring system and refining automated assembly processes to facilitate efficient large-scale production. Such advancements will contribute to improving the overall performance, scalability, and applicability of hybrid timber flooring solutions in modern construction practices.

Overall, this study also offers practitioners an initial framework for design. The workflow delivers valuable insights into joint performance when applying current wood industry technologies. The iterative processes of prototyping, testing, and evaluating key factors enable adjustments to the original design based on empirical data. Furthermore, the workflow outlines the full design iteration cycle, guiding practitioners on how to assemble multidisciplinary teams and set realistic expectations when developing new digitalized carpentry joints for applications beyond composite flooring systems. This study demonstrates the effectiveness of the workflow, highlighting its relevance to industry practices and its potential for broader implementation in the evolving digital construction environment.

7 – REFERENCES

[1] H. Kagermann, Lukas, W-D, Wahlster, W. “Industrie 4.0: Mit dem Internet der Dinge aufdem Weg zur 4.” Industriellen Revolution. (2011).

[2] "LIGNA 2015 AGAIN A TOP FAIR EDITION," Pro Ligno, vol. 11, (2015), pp. 52-53.

[3] S. A. Landscheidt, & M. Kans, *Automation Practices in Wood Product Industries: Lessons learned, current Practices and Future Perspectives*. (2016).

[4] A. Kunic, R. Naboni, A. Kramberger & C. Schlette. “Design and assembly automation of the Robotic Reversible Timber Beam.” *Automation in Construction*, *123*, (2021), 103531.

[5] N. H. P. L. Rogeau. “Robotic Assembly of Integrally-Attached Timber Plate Structures: From Computational Design to Automated Construction.” PhD thesis. EPFL. (2023).

[6] Intelligent-city. http://intelligent-city.com/(2025).

[7] Hundegger. https://www.hundegger.com (2025).

[8] Biesse. https://biesse.com/ww/en/machines-wood/ (2025).

[9] Techno Wood. https://www.technowood.swiss/en/ (2025).

[10] Hundegger. https://www.hundegger.com/en-ca/maschines/panel-processing-machines/pba-industry(2020)

[11] K. Orlowski. “Automated manufacturing for Timber-Based Panelised Wall Systems.” *Automation in Construction*, 109, (2020) 102988.

[12] HOMAG. https://www.homag.com/en/ (2025)

[13] Y. Diao & C. Loss. “Long-Span CLT-Glulam Composite Flooring System Connected with Bamboo-Based Shear Connectors: Feasibility of Design for Assembly.” In *Canadian Society of Civil Engineering Annual Conference*. (2022), pp. 333-348.

[14] Canadian Standards Association. *CSA O86-19: Engineering design in wood.* (2019).

[15] American National Standards Institute & APA – The Engineered Wood Association. *ANSI/APA PRG 320: Standard for performance-rated cross-laminated timber*. (2018).

[16] Canadian Standards Association. *CSA O122-16: Structural glued-laminated timber*. (2016).

[17] Y. Diao & C. Loss. “Feasibility Study on Long-Span CLT-Glulam Composite Flooring System Connected with Bamboo-Tenon Shear Connectors.” In *13th World Conference on Timber Engineering.* (2023), pp. 3439-3448.

[18] MOSO International B.V. www.moso-bamboo.com (2025)

[19] R. Brandner, T. Bogensperger and G. Schickhofer. “In plane hear Strength of Cross Laminated Timber (CLT): Test Configuration, Quantification and Influencing Parameters.” In *CIB World Congress*. (2013).

[20] ASTM International. “Standard Test Methods for Mechanical Fasteners in Wood (ASTM D1761-20).” (2020).

https://doi.org/10.52202/080513-0149